EFFECTS OF SALINITY ON SOLID PARTICLE SETTLING VELOCITY IN NON-NEWTONIAN HERSCHEL – BULKLEY FLUIDS

An Undergraduate Research Scholars Thesis

by

SYEDA MANAHIL AKHTER, ANURAG SRIVASTAVA, and HADEAR HASSAN

Submitted to the Undergraduate Research Scholars program at
Texas A&M University
in partial fulfillment of the requirements for the designation as an

UNDERGRADUATE RESEARCH SCHOLAR

Approved by Research Advisors: Dr. Ibrahim G. Hassan
Dr. Aziz Rahman

May 2020

Major: Mechanical Engineering

TABLE OF CONTENTS

Page

ABSTRACT 1

ACKNOWLEDGMENTS 3

NOMENCLATURE 4

CHAPTER

I. INTRODUCTION 5

Rheology of Fluids 5
Settling Velocity of Particles 14

II. METHODS 19

Equipment 19
Procedure 22

III. RESULTS 24

Surface Tension 24
Spherical Particle in Newtonian Fluid 25
Spherical Particle in Non-Newtonian Fluid 28
Non-spherical Particle in Non-Newtonian Fluid 34

IV. CONCLUSION 40

REFERENCES 42

ABSTRACT

Effects of Salinity on Solid Particle Settling Velocity in Non-Newtonian Herschel – Bulkley Fluids

Syeda Manahil Akhter, Anurag Srivastava, and Hadear Hassan
Department of Mechanical Engineering
Texas A&M University

Research Advisor: Dr. Ibrahim G. Hassan
Department of Mechanical Engineering
Texas A&M University

Research Advisor: Dr. Aziz Rahman
Department of Petroleum Engineering
Texas A&M University

The purpose of this thesis research is to have a fundamental understanding of the behavior of particles in Non-Newtonian Herschel-Bulkley Fluids. Settling velocity or depositional velocity is a critical parameter in drilling technology, and hydrocarbon processing as the non-settling condition of particles depends on it. Also, understanding the settling velocity of a Newtonian fluid with high salinity will help for better separation of oil and natural gas streams in processing facilities.

There are limited studies available in the literature for Herschel-Bulkley (H-B) fluid with salinity. In this study, we measure the fluid rheology of non-Newtonian Herschel-Bulkley (H-B) fluid with and without salinity. Experiments were conducted to measure the settling velocity of a particle in different salinity conditions. From experimental results, settling velocity characteristics with changing salinity in drilling fluids will be found. In Qatar's grand challenges, it is indicated that energy should be produced efficiently. Fundamental understating of non-

depositional velocity in drilling and other hydrocarbon processing will assist in efficient hydrocarbon recovery in Qatar.

Data from previous research for the Undergraduate Research and Entrepreneurship program was used to present the new findings. From experiments, it was found that the settling velocity of particles increases with increasing size of the particles. A power relationship was established between the collected data for the drag coefficient and Reynold's number. Increasing the salt concentration increased the settling velocity of the particles. Also, as sphericity of particles increases, the settling velocity increases. Plans were made to determine the relationship between surface tension and the settling velocity of particles in non-Newtonian fluids. However, due to COVID-19, labs were closed, and hence experiments were not completed. Larger column experiments were not carried out for this reason. In the future, a paper will be submitted to the ASME International Mechanical Engineering Congress & Exposition 2020 and showcase the efforts made to fill the gap in the research for the modeling of the behavior of non-Newtonian fluids.

ACKNOWLEDGMENTS

The authors gratefully acknowledge the opportunity provided by the Undergraduate Research and Entrepreneurship program (project no. UREP 23-131-2-044) and the financial support of the Qatar National Research Fund in the duration of this project. The student authors also give a great appreciation of Dr. Ibrahim Hassan, Dr. Aziz Rahman, Dr. Fahed Qureshi & Mr. Hicham Ferroudji from Texas A&M University at Qatar for their guidance and wisdom.

NOMENCLATURE

d	Particle diameter
H-B	Herschel-Bulkley fluid model
K	Flow consistency index [$Pa.s^n$]
n	Flow behavior index [dimensionless]
Re	Reynolds number
V^*	Shear velocity
V_t	Terminal settling velocity
γ	Shear rate [1/s]
ρ_l	Liquid density
ρ_s	Settling particle density
τ	Shear stress [Pa]
τ_0/τ_y	Yield stress [Pa]
V_b	Bulk volume [cm^3]
D	Core diameter [cm]
L	Core length [cm]
Q	Flow rate [cm^3/min]
k_l	Liquid permeability [mD]
A	Area [cm^2]
P	Pressure [psi]

CHAPTER I

INTRODUCTION

Rheology of Fluids

Fluids are separated into two main rheological categories. The two categories are Newtonian and Non-Newtonian fluids. A non-Newtonian fluid's viscosity varies based on applied force and stress. The physical properties of non-Newtonian fluids are depending on the forces acting on it during a specific time. Based on several research papers, it can be concluded that a non-Newtonian fluid has flow properties that are described as different constant values of viscosity. A majority of fluids are Non-Newtonian such as paint and starch suspensions. Contrarily to a Newtonian solution which has a linear relationship between strain rate and shear stress, Non-Newtonian fluids have a non-linear relationship, as seen in Figure 1. It can also be time-dependent.

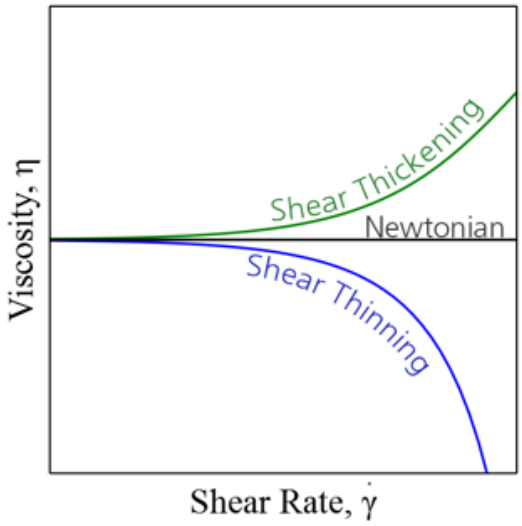

Figure 1: Viscosity of Newtonian, shear-thinning, and shear thickening fluids as a function of shear rate [1].

A Non-Newtonian fluid does not follow Newton's law of viscosity. This law states that there is a constant viscosity which is independent of stress. Most liquids in real life are Non-Newtonian. Non-Newtonian fluid's viscosity can change when they are exposed to stress. The viscosity of such fluids depends on the shear rate or the deformation history.

Non-Newtonian fluids are also categorized into three main subcategories: viscoelastic fluids, viscous fluids, and time-dependent fluids. Viscoelastic fluids are additionally divided into four other categories: shear thinning, shear thickening, Bingham, and Herschel Bulkley (HB) fluids [2]. The two initial fluid types are known as Power-Law fluids. The two others exhibit initial yield stress that needs to be overcome prior τ_0. Figure 2 shows the respective τ vs. $\dot{\gamma}$ relationships [3]:

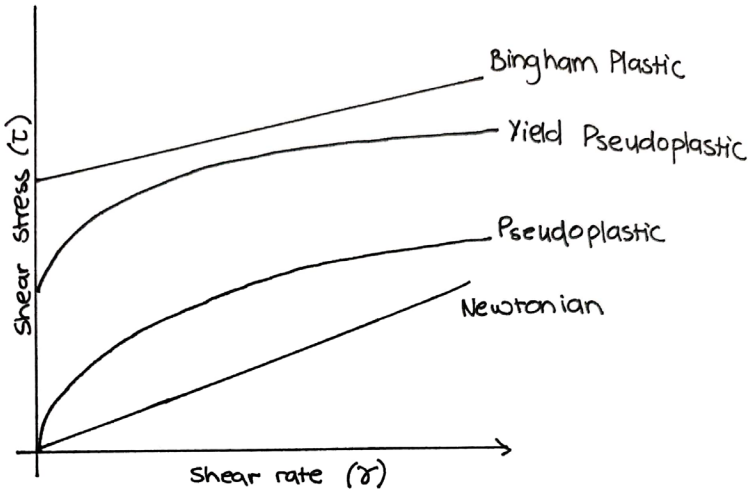

Figure 2: Typical rheological models on shear stress vs. shear rate plot adapted from [3].

The equation demonstrated below was developed for HB Fluids [4]:

$$\tau = \tau_o + K\dot{\gamma}^n \quad (1)$$

In Equation 1, *K* is the fluid consistency index, and n is the behavior index. If the initial yield was taken to be zero, Equation 2 could be used. Equation 2 is the Power-Law model.

$$\tau = K\dot{\gamma}^n \quad (2)$$

For this model, if the fluid behavior index, n, is $(n < 1)$, a shear-thinning behavior can be observed. On the other hand, for $n > 1$, shear thickening is observed. Lastly, a fluid with $n = 1$ but with an initial yield produces the Bingham model. Equation 3 can be used in this case.

$$\tau = \tau_o + PV(\dot{\gamma}^1) \quad (3)$$

In the case of the Bingham model, the plastic viscosity (PV) is what was initially the proportionality constant. A paper by Amani et al. [4] studied the effects of salinity on drilling fluids. The study used two salts, NaCl and KCl, as the test components. The composition of the drilling mud used for the study is presented in Table 1.

The study that was conducted tested two components, which were two salts: NaCl and KCl. Table 1 shows the composition of the drilling mud that was used for the mentioned research.

Table 1: Table of composition for studied mud [4].

Additives	[PPB]
Water	268.61
M-I Gel Supreme	8.00
Caustic Soda	1.00
Asphasol Supreme	5.00
XP-20	5.00
Black Fury	5.00
Lime	2.00
DRISCAL	5.00
POROSEAL	10.50
SAFE SCAV HS	0.40
Barite	214.49

Three different compositions were then taken from each of the two salts. The three compositions were 3 wt%, 5 wt%, and 7 wt%. They were then studied under a multitude of cases: from 0 MPa to 241 MPa (from 0 psi to 35,000 psi) with 34 MPa (5,000 psi) increments and from 21°C to 232 °C (from 70°F to 450°F) with 13 °C (56°F) gradations [4]. Figure 3 shows

the resulting shear rate/stress diagrams for the two salts. Figure 3 shows the resulting shear rate/stress diagrams for high pressure and high temperature (HPHT) conditions.

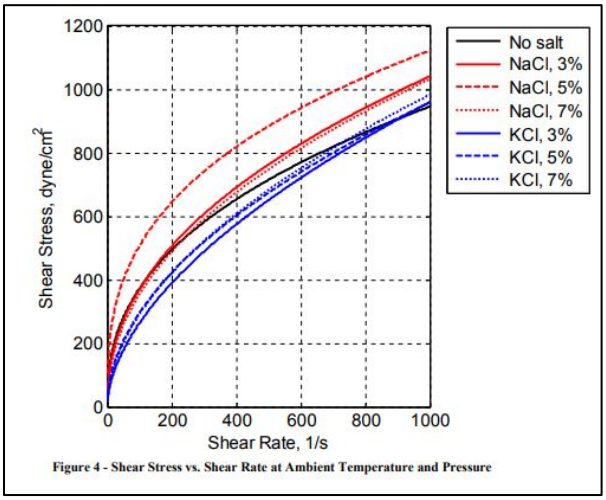

Figure 3: Varying salt concentrations at ambient pressure [4].

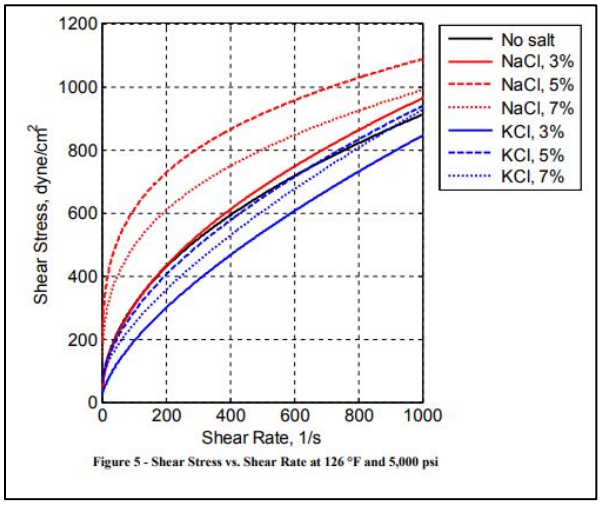

Figure 4: Varying salt concentrations at 52 ºC (126 ºF) & (34 MPa) 5,000 psi [4].

From Figures 3 and 4, it can be seen that with the increase of NaCl presence, there is an increase in the shear stress per shear rate. On the other hand, with an increase of KCl, there is an observed decrease in the same relationship. It is assumed that NaCl increases the thickening behavior of the fluid, while KCl gives a thinning behavior of the fluid. It was also observed that HPHT conditions generate a more significant range between different concentrations of the salt.

This indicates that the wt% of salt has more influence on the shear stress in bottom hole conditions. Bottom hole conditions are at higher pressure. At higher pressure, the fluid may exhibit thickening behavior, and thus, higher stress is needed.

It was indicated that the HB model was the best fitting for saline-ingested drilling fluid, with the coefficient of determination nearing an average of $R^2 = 0.986$. Anawe & Folayan [5] recently published a report presenting advances in drilling fluid rheology. This was indicated by statistical analysis of a variety of models on various types of muds, as well as on water-based muds (WBMs). An automatic eight speeds viscometer model 800 was used by the research team. The WBM was prepared with components and compositions shown in appendix A&B and under standard procedures recommended by the American Petroleum Institute. Table 2 shows the readings for the WBM.

Table 2: Viscometer readings for water-based mud [5].

Speed (RPM)	Dial Reading (lb/100ft^2)	Shear Rate (s^{-1})
600	88	1022
300	60	511
200	45	340.60
100	33	170.30
60	25	102.18
30	19	51.09
6	15	10.22
3	12	5.11

The research also applied different rheological models on the data set obtained in the experiment. The overlaying of all these models with their respective abbreviations can be observed in Figure 5. The conclusion is that the most-statistically accurate model for predicting the rheological behavior is the Casson rheological model (CRM).

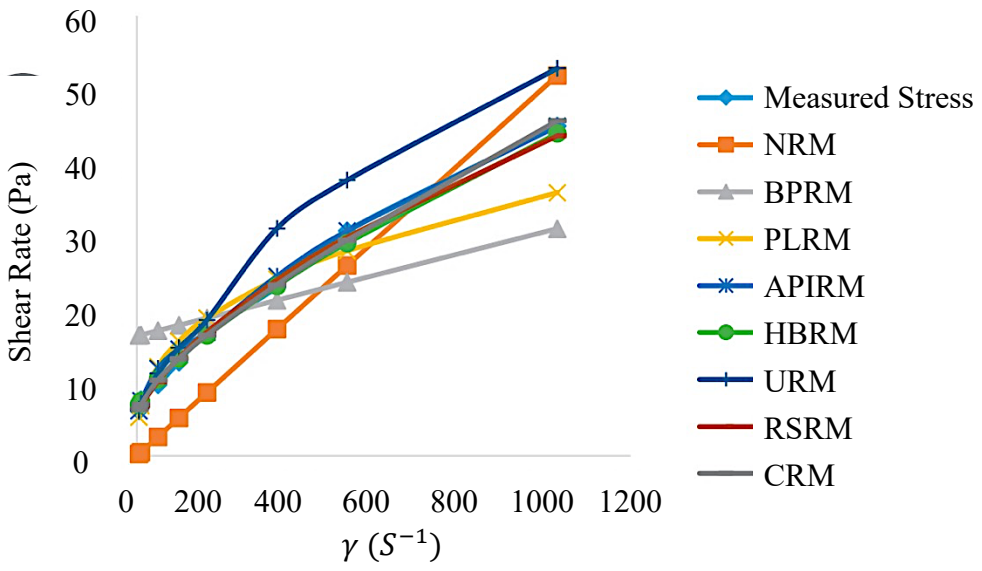

Figure 5: Varying models compared to true measured stress on shear stress vs. shear rate plot [5].

Figure 5 represents the comparison of the experimental results and different rheological models.

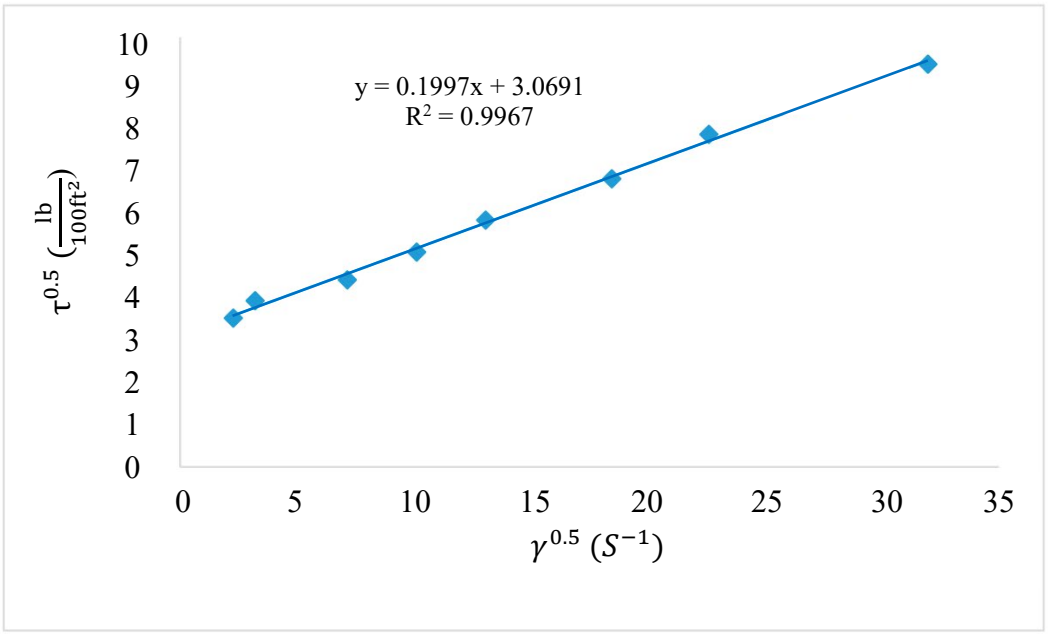

Figure 6: Casson rheological dataset on shear stress vs. shear rate plot [5].

The most effective model in predicting the rheology was deduced to be the Casson Rheological. Through the use of the coefficient of determination (R^2) similar to Amani et al. [4],

the prediction of the rheology of a simple WBM as per composition in Appendix A of the API procedures, yielded a value of $R^2 = 0.9967$ as seen in Figure 6 [5]. In addition, it can be observed that the Bingham plastic or Newtonian model least-effectively represents the rheology of WBMs. The Herschel-Bulkley model – the model used for this studies' rheological experimentation was found to be the most effective model at predicting the rheology of WBMs because it describes the behavior accurately at low and high shear rates.

Data from previous research conducted on "Effects of Salinity on Solid Particle Settling Velocity in Non-Newtonian Herschel–Bulkley Fluids" by Robert Moukhametov, Jerahmeel Bautista and two of the authors from this research; Syeda Akhter and Anurag Srivastava for their Undergraduate Research and Entrepreneurship Program, were used to present the new findings. From that research, Figure 7 was obtained, which presented the shear stress for two non-Newtonian fluid with 0.1 wt% Flowzan and 0.2 wt% Flowzan.

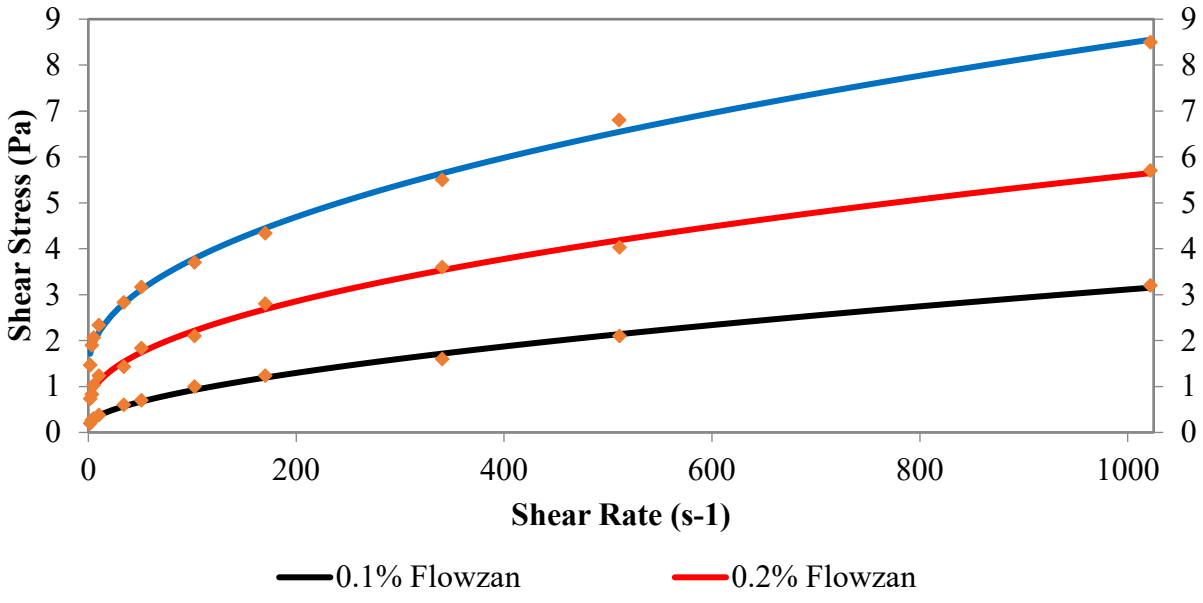

Figure 7: Flowzan variation shear stress vs. shear rate.

It was deduced that viscosity increases with increasing Flowzan concentration, which in turn causes the yield stress to increase. The data points obtained were found to follow the HB

model, as shown in Equation 1. In addition, the effect of adding NaCl salt to the Flowzan fluid was investigated. Figure 8 shows the shear stress values plotted for 0.1 wt% Flowzan with three different concentrations of NaCl salt. Similarly, Figure 9 shows the shear stress values but for fluids with 0.2 wt% Flowzan and NaCl salt.

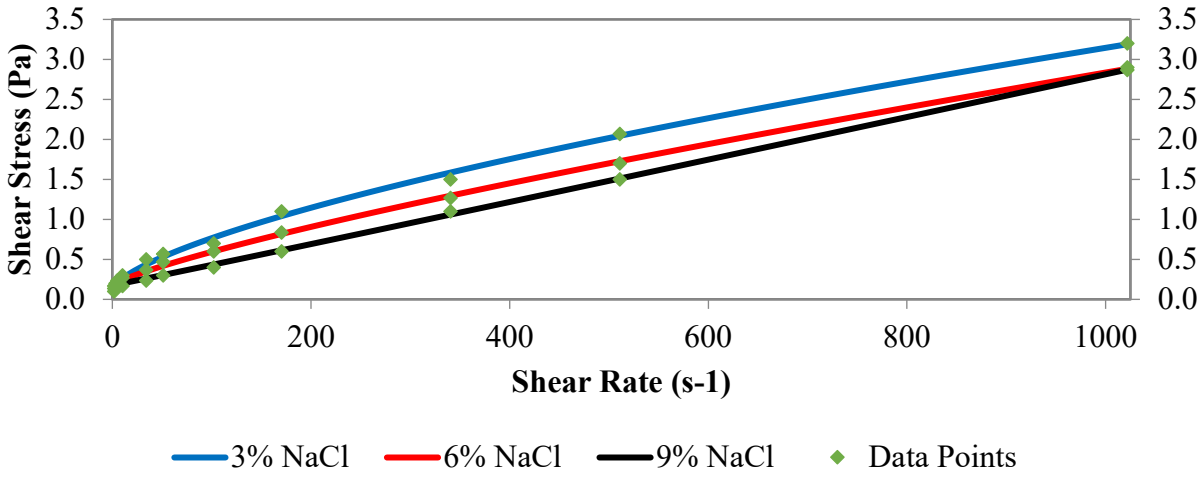

Figure 8: 0.1 wt% Flowzan with NaCl variation shear stress vs. shear rate.

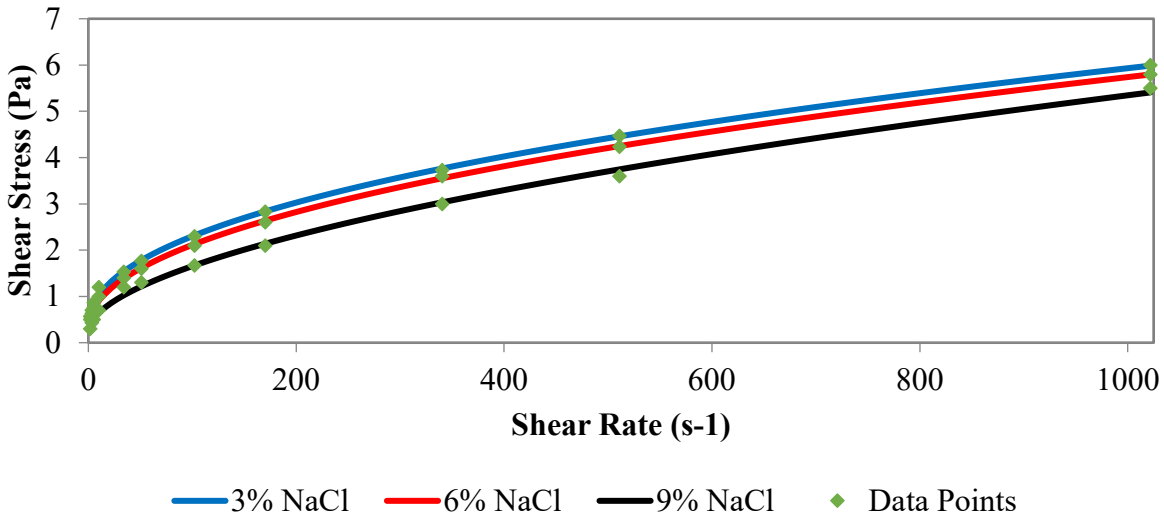

Figure 9: 0.2 wt% Flowzan with NaCl variation shear stress vs. shear rate.

It was observed that as NaCl concentration increases, the shear stress for a particular shear rate decreases. The trend observed from the 0.2 wt% Flowzan graph shows that the data points follow the HB model more closely, meaning that Flowzan plays the dominant role in the

characteristic of the fluid. The research was also conducted with varying calcium chloride salt concentrations. Figure 10 and Figure 11.

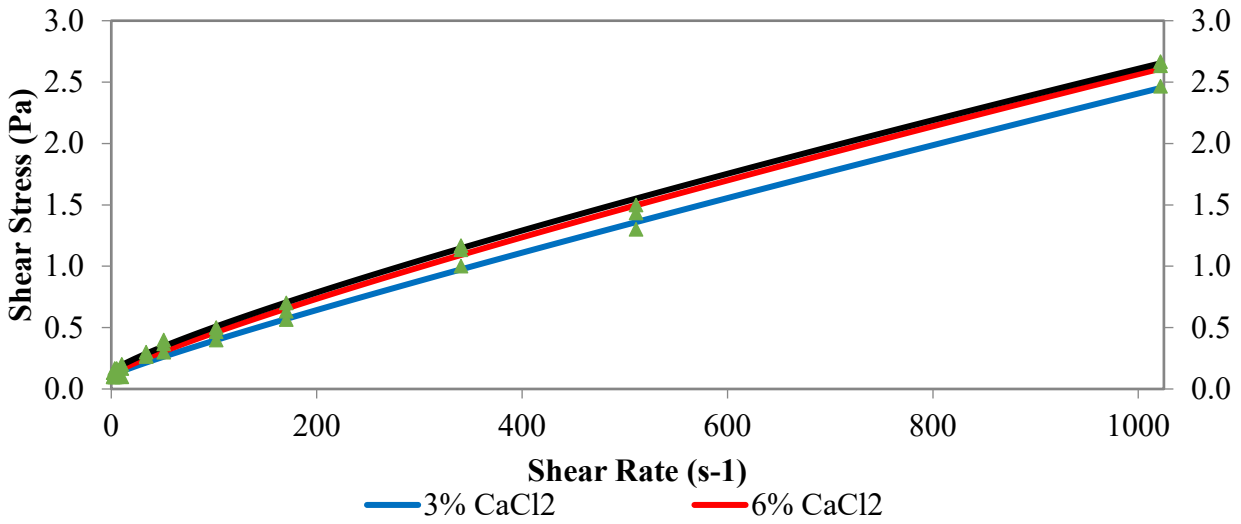

Figure 10: 0.1 % Flowzan with $CaCl_2$ variation shear stress vs. shear rate.

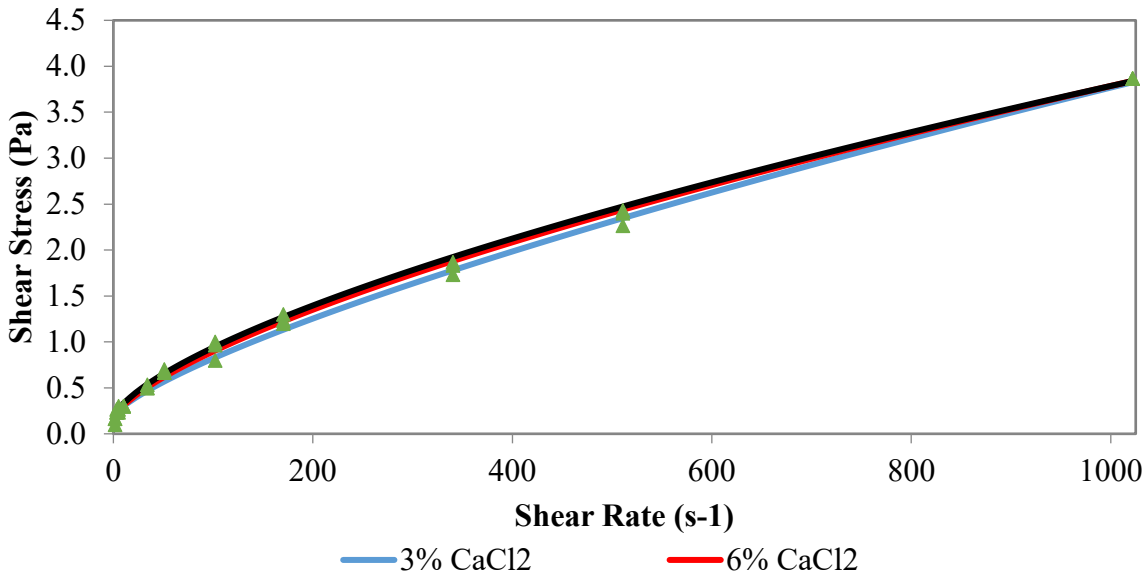

Figure 11: 0.2 % Flowzan with $CaCl_2$ variation shear stress vs. shear rate.

It was observed that as the concentration of calcium chloride increases, the shear stress for a particular shear rate also increases. The data from the graphs and the raw data from this research will be used in our experiment to present our findings.

The conclusions from the rheology literature review can be summarized as follows:

1. The increase in the concentration of NaCl led to a decrease in the shear stress of the fluid.
2. There was an increase in shear rates observed for higher Flowzan concentrations.
3. Flowzan concentration was more dominant than the NaCl concentration on the rheology of the fluid.
4. A slight increase in shear stress was observed when the concentration of $CaCl_2$ was increased for a constant shear rate.
5. Irrespective of the Flowzan concentration, the shear rate variation of the solution was negligible for different $CaCl_2$ concentrations.
6. For lower Flowzan concentrations, $CaCl_2$ salt modified the model to a Bingham Plastic model from the Herschel-Bulkley model.

Settling Velocity of Particles

The settling velocity of an object is defined as the velocity that an object moves in a fluid with when the force due to gravity nullifies the resistive drag force against it. As the object accelerates and its velocity increases, the drag force acting on the object also increases. The velocity at which the drag force has increased to equals the force of gravity, which is considered as settling velocity [6].

Various industrial applications such as geothermal drilling, water waste processing, drilling of oil and gas wells require excellent knowledge of the terminal settling velocity of a solid in a liquid. The settling velocity of a particle through a fluid is dependent on many factors, such as the particle size, shape, particle grain size, and the density of the settling medium. A paper published in May 2008 about the measurement and modeling of the settling velocity of isometric particles by Hazzab Abdelkrim et al. [7] defined a dimensionless number on the

particle properties like shape and flow characteristics. The relationship between the number and the Archimedes number can be used to derive a model for the settling velocity.

A numerical method was developed in another study regarding settling velocities of particles to validate the experimental data [8]. However, this model had its limitations since it was done only for a one-dimensional setup. From this study, the authors were able to conclude that sedimentation and consolidation behavior in particles could be represented using the phenomenological theory for flocculated slurries. Furthermore, there is no universal model that is used, but models are modified depending on the fluid properties and then validated by conducting experiments.

Non-spherical Particles

Particles are not perfect spheres but irregular 3-D objects with non-uniform sphericity, smoothness, and circularity, which correlates with the value of the drag coefficient. Furthermore, their shape complicates the calculations made to determine parameters like the drag coefficient. One method to simplify this problem is to assume the irregular particle to be a sphere of equivalent diameter. However, this assumption might decrease the accuracy of the results due to the ignorance of phenomena such as light scattering, which can affect the shape of the particle.

From literature, researchers have found few ways to determine the equivalent diameter of these particles. The diameters that can be derived from these methods are the Feret diameter and the projected area diameter. Figure 12 shows the difference between the two diameters, and these diameters can be obtained using techniques such as laser obscuration time (LOT) and image analysis [9]. LOT uses laser beams that revolve at a high frequency around the particle, which creates a pulse. The pulse duration is used in conjunction with a photodiode to record the time for which the particle has blocked the path of the laser [10].

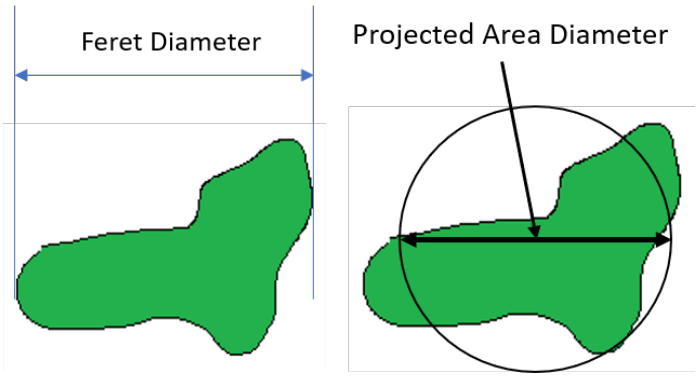

Figure 12: Examples of Feret and projected area diameter of a particle [9].

From the literature review, the main conclusions considered when conducting experiments are as follows:

1. Spherical particles have higher settling velocities when compared to non-spherical particles.
2. Particles flowing in denser fluids have a higher settling velocity than less dense fluids.
3. Settling velocity and particle sphericity are directly proportional.
4. The orientation of the non-spherical particles while falling affects the terminal settling velocity of the particle.

From the literature review, it was determined that little research had been performed with Herschel Bulkley fluids, which is the primary focus of this study. Due to the lack of experimental models in literature for settling velocity, the objective of this study is to determine the settling velocity of spherical and non-spherical particles in Herschel-Bulkley fluids and compare the data obtained with the existing models found in the literature.

Theory

In order to determine the time required for a solid to settle down in a complex non-Newtonian fluid, it is essential to understand the shape of the solid [11]. From the literature

review, it was determined that the key parameters, which will be needed to calculate, are Reynold's number (Re) and the drag force coefficient (C_D) [11]. The Reynold's number is defined as the ratio of the internal forces experienced on fluid due to the viscous forces. In the case of a stationary fluid, Reynold's number is mathematically shown in Equation 4.

$$Re = \frac{dV_{ts}\rho_l}{\mu_l} \tag{4}$$

Where d is the diameter of the solid, V_{ts} is a velocity of the particle, ρ_l is density and μ_l is the viscosity. On the other hand, the drag coefficient is defined as the resistance of an object in a fluid environment such as water, air, or drilling mud. Mathematically, it is shown in Equation5.

$$C_D = \frac{4(\rho_s - \rho_l)dg}{3{V_{ts}}^2\rho_l} \tag{5}$$

Equation 6 represents the drag force, F [12]. This force will have to balance the force due to gravity, for the particle to reach settling velocity.

$$F = \frac{\pi}{6}d^3(\rho_s - \rho) \tag{6}$$

$$\tau = \tau_0 + K(\gamma)^n \tag{7}$$

$$\mathrm{Re}^*_{HB} = \frac{d^n(V^*)^{2-n}\rho_l}{\tau_0\left(\frac{d}{V^*}\right)^n + K} \tag{8}$$

Terminal settling velocity determination is very critical in determining Reynold's number and the drag coefficient. From literature, for Newtonian fluids, the most accurate C_D vs. Re relations have been identified by the formulas that have been proposed by Cheng (Equation 9) for subcritical regions [13]. The drag coefficient for the experimental data was also determined using Equation 10 [13]. In both cases, Reynold's number was determined using Equation 11.

$$C_{ds} = \frac{24}{Re_s}(1 + 0.27Re_s)^{0.43} + 0.47[1 - \exp(-0.04{Re_s}^{0.38})] \tag{9}$$

$$C_D = \frac{4(\rho_s - \rho_l)dg}{3{V_{ts}}^2\rho_l} \tag{10}$$

$$Re = \frac{dV_{ts}\rho_l}{\mu_l} \quad (11)$$

It is important to note that Equations 4 and 5 are valid in the case of Newtonian fluids [14]. In the case of Non-Newtonian fluids, these equations must be modified with the usage of the Herschel-Bulkley rheology equation and replacing the dynamic viscosity term with apparent viscosity. The apparent viscosity is evaluated at a shear rate equal to the ratio of the terminal velocity (V_{ts}) and the particle diameter (d). The shear stress and modified Reynold's number for non-Newtonian fluid are expressed as follows:

To find the drag force exerted by a particle, relationships between C_D vs. Re_ρ will be observed graphically. Previous efforts to generate an explicit method to determine V_{ts} have been made by modifying the C_D vs. Re_ρ (Wilson method). Although the Wilson method is an explicit method to determine the terminal velocity, there is a limitation to this method, which is that there is high uncertainty (75% and above) in the predicted values of terminal velocity using this method [15]. Through the literature, there have been different modified models of the Wilson method, which have tried to yield accurate results for non-Newtonian fluids [15]. The first model is represented in Equation 12 and Equation 13, which was proposed by Kelessidis and Mpandelis [12]. Equation 14 shows the drag coefficient equation, which was proposed by Margaritis et al. [16].

$$C_D = [2.25 * Re^{-0.31} + 0.36 * Re^{0.06}]^{3.45} \quad 1 < Re < 1000 \quad (12)$$

$$C_D = \frac{24}{Re} + \frac{4}{\sqrt{Re}} + 0.4, \; Re < 10^5 \quad (13)$$

$$C_D = \frac{4\Delta\rho d_e^3 g}{3{U_t}^2 \rho} \quad (14)$$

CHAPTER II

METHODS

Equipment

The equipment used for experimentation is as follows:

1. *Fann* Hamilton Beach Mixer Model HMD200 (Figure 13)

Figure 13:Fann Hamilton Beach Mixer Model HMD200.

2. MIKROTRON high speed camera (10 - 30 V DC, 15 Watts) and Velbon tripod for the camera (Figure 14)

Figure 14:MIKROTRON High Speed Camera and Velbon tripod.

3. Measuring cylinder
4. Glass beaker

5. Funnel

6. Two Dedolight High Intensity Lamps (Figure 15)

Figure 15:Dedolight High Intensity Lamps.

7. 2 Acrylic columns (Total height = 75 cm, Rectangular cross-section) (Figure 16 and Figure 17)

   - 1st column has a section of 7.5 cm by 7.5 cm
   - 2nd column has a section of 15.2 cm by 15.2 cm

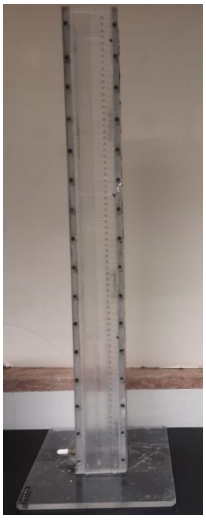

Figure 16:Acrylic column smaller cross-section.

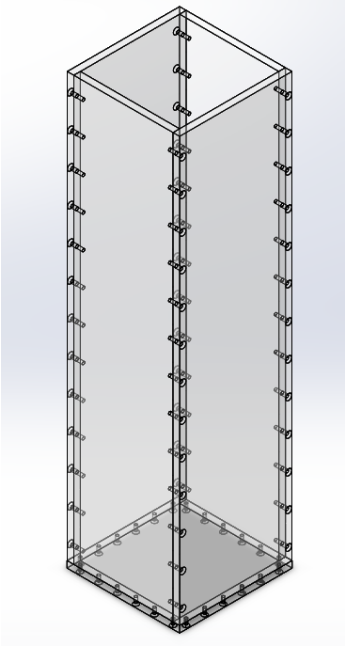

Figure 17:Acrylic column larger cross-section.

8. White cardboard for background

9. Digital Mass Balance (1E-3 g accuracy) (Figure 18)

Figure 18: Weighing the 0.1 wt% Flowzan.

10. NaCl > 99.5% Salt

11. $CaCl_2$ > 99.5% Salt

12. Flowzan

13. Supplementary equipment (measuring plates, beakers, stirring rods)

Please note that most of the equipment was available at the lab during the time of the project except for the larger acrylic column. The column was designed on SolidWorks, as shown in Figure 17. The manufacturing process for the larger column was due to start in March. However, due to the unforeseen circumstances that arose with the measures taken to limit the spread of COVID-19, the larger column could not be manufactured. The purpose of this column was to conduct settling velocity experiments in order to check if there was any wall-effect that could have affected the results that were generated with the usage of the smaller column.

Procedure

The procedures for making the non-Newtonian fluids is as follows:

1. Use the beaker to measure 250 ml of water and pour it into a mixing cup.
2. Use the digital mass balance to measure out 0.1 wt% of Flowzan (0.25 g) and put it in the mixing cup containing the water (Figure 18).
3. Turn on the mud mixer to the lowest setting and mix it for 5 minutes.
4. Turn the mixer off and use the glass rod to remove the Flowzan deposited on the sides of the mixing cup.
5. Turn the mud mixer on the lowest setting again and mix for another 10 minutes.
6. Using the mass balance, measure out the 3 wt% (7.5 g) of sodium chloride (NaCl) salt.
7. Gradually pour the salt into the mixing cup and mix for an additional 10 minutes.
8. Repeat the process until 3 liters of fluid is made.
9. Pour the fluid in the testing column until fluid reaches the 60 cm mark.
10. Turn on the lamps and set up the camera.
11. Start the camera and drop the required particle.

12. Export the recording for analysis.

13. Repeat the process of making the fluid and testing with the other fluids shown in Table 3.

Table 3: Sample concentration variations.

Sample	Flowzan [wt. %]	NaCl [wt. %]	$CaCl_2$ [wt. %]
1	0.1	no salt	no salt
2	0.2	no salt	no salt
3	0.3	no salt	no salt
4	0.1	3	no salt
5	0.1	6	no salt
6	0.1	9	no salt
7	0.2	3	no salt
8	0.2	6	no salt
9	0.2	9	no salt
10	0.1	no salt	3
11	0.1	no salt	6
12	0.1	no salt	9
13	0.2	no salt	3
14	0.2	no salt	6
15	0.2	no salt	9

CHAPTER III

RESULTS

Surface Tension

The surface tension was measured for 12 fluids with different concentrations of NaCl and Flowzan. It was calculated using a Sigma Tensiometer, which is a high-performance device for measuring surface tension with the use of a Wilhelmy plate. The first step was to obtain the densities of the fluid, using a graduated cylinder and a scale. These values were computed in the tensiometer before calculating the surface tension. The next step was to calibrate the tensiometer and hang the Wilhelmy plate on edge. The plate was then displaced vertically until it was in contact with the liquid. The measurement was read from the screen displayed on the machine, once a clear meniscus was shown on the plate. Table 4 shows the measurement of three different runs of the experiment on each liquid.

Table 4: Surface tension measurement.

Samples	Flowzan	NaCl	Density (g/ml)	Surface 1 (mN/m)	Surface 2 (mN/m)	Surface 3 (mN/m)
1	0.1	no salt	1.0522	54.36	53.92	53.67
2	0.2	no salt	1.049	53.17	54.15	50.27
3	0.3	no salt	1.0423	57.2	61.2	60.4
4	0.1	3	1.0657	53.4	49.3	52.5
5	0.1	6	1.072	52.4	51.2	54.3

The possible sources of error for this experiment are the presence of bubbles in the liquid and the Wilhelmy plate. The presence of bubbles interferes with the measurement of both the density and surface tension. To prevent the presence of bubbles, the liquids were set overnight on a magnetic stirrer. Small bubbles were still present during experimentation. The next possible source of error was the overuse of the Wilhelmy plate. In order for the data to be accurate, the

Wilhelmy plate had to be straight with no bending, yet with the overuse, it caused the material to have very slight bends.

Spherical Particle in Newtonian Fluid

The experiments for settling velocity were first carried out with a Newtonian fluid (water) using three black glass spheres of diameters 9.53 mm, 6.53 mm & 4.76 mm. The parameters of the sphere balls are shown in Table 5.

From the experimental data, a series of graphs were created. Figure 19 shows the instantaneous velocity versus time graph for the 9.53 mm diameter black glass sphere in water. While calculating the instantaneous velocity, it was considered that the time between each frame generated by the camera was small enough to determine the instantaneous velocity.

Table 5: Parameters of the glass sphere balls.

Diameter (mm)	Area (m^2)	Volume (m^3)	Mass (g)	Weight (N)	Buoyancy Force (N)	Drag Force (N)
9.53	7.133×10^{-5}	4.53×10^{-7}	1.449	0.01421	0.004584	0.009631
6.53	3.349×10^{-5}	1.46×10^{-7}	0.358	0.00351	0.001475	0.002037
4.76	1.780×10^{-5}	5.65×10^{-8}	0.145	0.00142	0.000571	0.000851

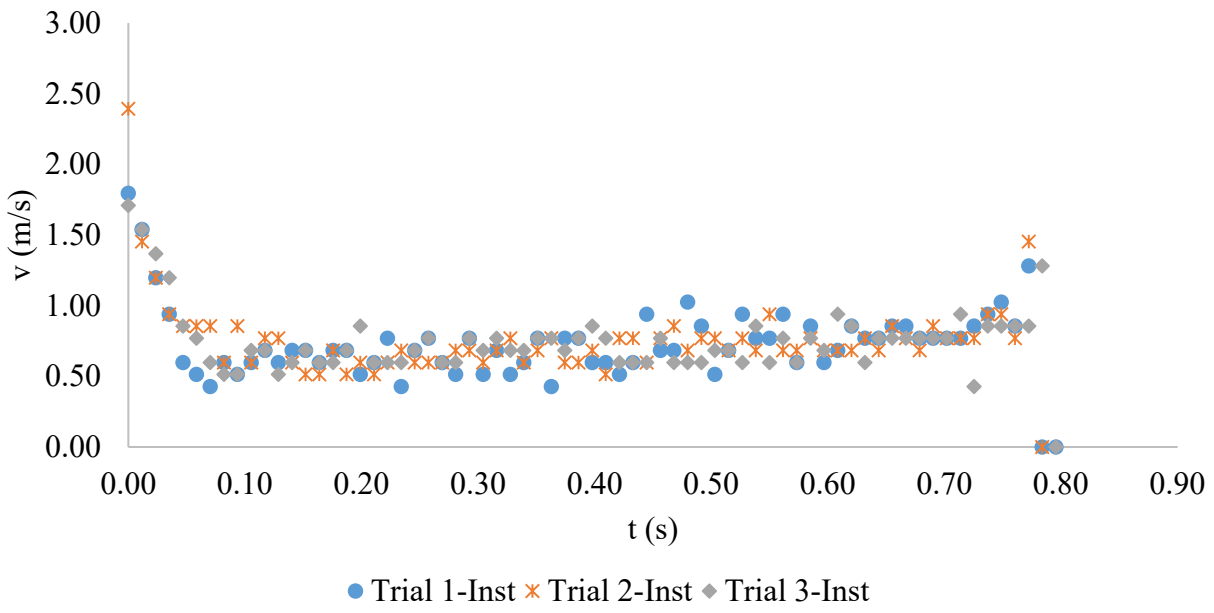

Figure 19: 9.53 mm diameter instantaneous velocity vs. time for water.

From Figure 19, it was observed that the spheres initially entered the water at a high velocity for all the trials. The particle had not been released at 60 cm (water height), but from the top of the column, therefore, the particle had a few centimeters before it touched the water. This meant that the particle had an initial velocity before it encountered the water. Following this, the velocity of the particle decreased due to the countering drag force from the water. Once there is no change in velocity with time, we can consider that the particle achieved terminal velocity. The data collected for the figure shows signs of repeatability as the different trials overlap each other. Variations in the data point may be due to the presence of small air bubbles in the fluid column. Using the properties of water at standard conditions, the coefficient of drag vs. Reynolds number graph was plotted, as seen in Figure 20.

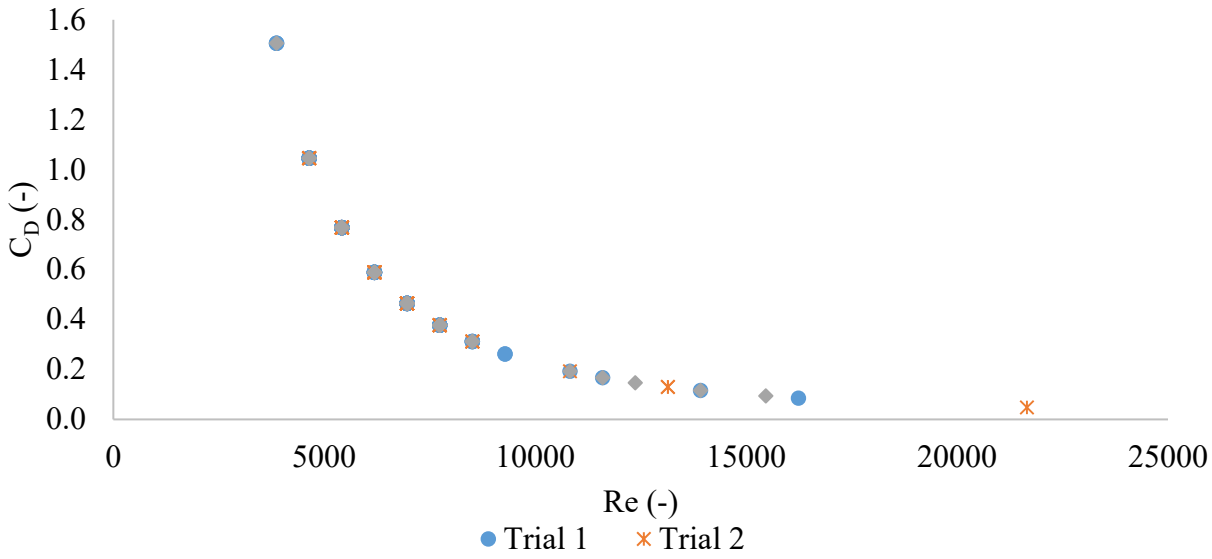

Figure 20: Coefficient of drag vs. Reynolds number graph for water.

Similarly, the instantaneous velocity was calculated as overtime for the 4.76 mm black glass sphere (Figure 21). It was again observed that the velocity initially was high and decreased rapidly, reaching terminal velocity. The terminal velocity was observed to be around 0.5 m/s. The data point for velocity in trial one towards the end that distant from the rest of the data was due to the sphere hitting the wall of the column. Another reason could be that the sphere possibly hit an air bubble. The C_D vs. Re graph, as presented in Figure 22, exhibits the same exponential decrease as found for the larger diameter sphere. The Reynold number range was lower for the smaller sphere as compared to the larger sphere.

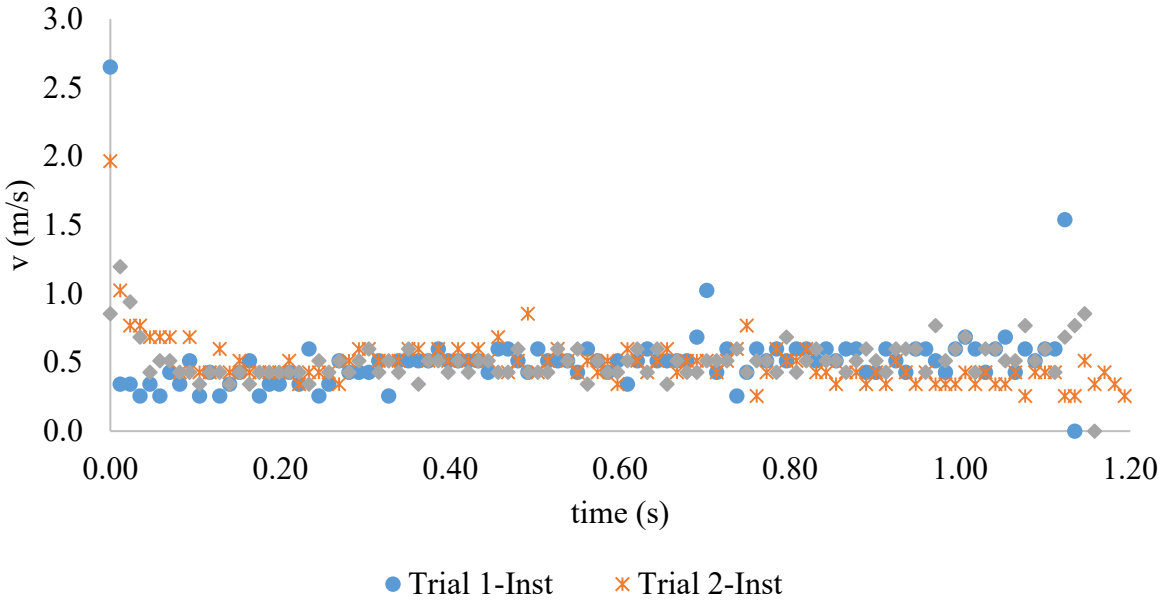

Figure 21: 4.76 mm diameter instantaneous velocity vs. time for water.

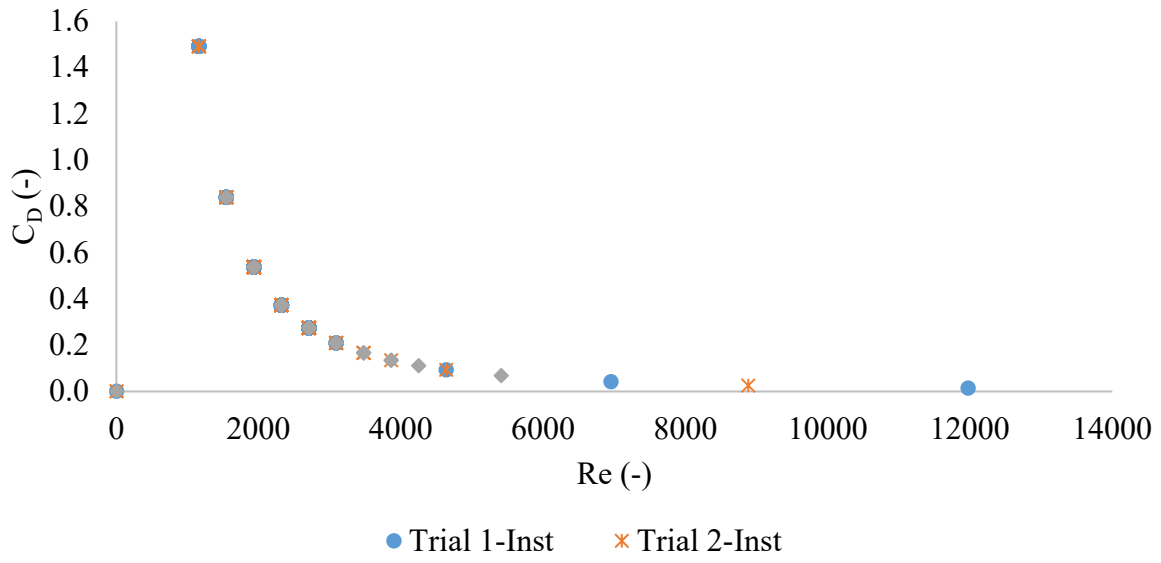

Figure 22: Coefficient of drag vs. Reynolds number graph for the 4.76 mm sphere in water.

Spherical Particle in Non-Newtonian Fluid

Following the experiments with Newtonian fluids, experiments were performed with non-Newtonian fluids, which contained a solution of Flowzan and sodium chloride salt. Figure 23 shows the instantaneous velocity vs. time graph for the 4.76 mm black glass sphere when dropped in 0.1 wt% Flowzan and 3 wt% NaCl fluid. From the graph, the terminal settling

velocity of the particle was determined to be approximately 0.43 m/s. In comparison to the settling velocity value of water, the velocity for this sphere was less due to the difference in viscosities of the two fluids.

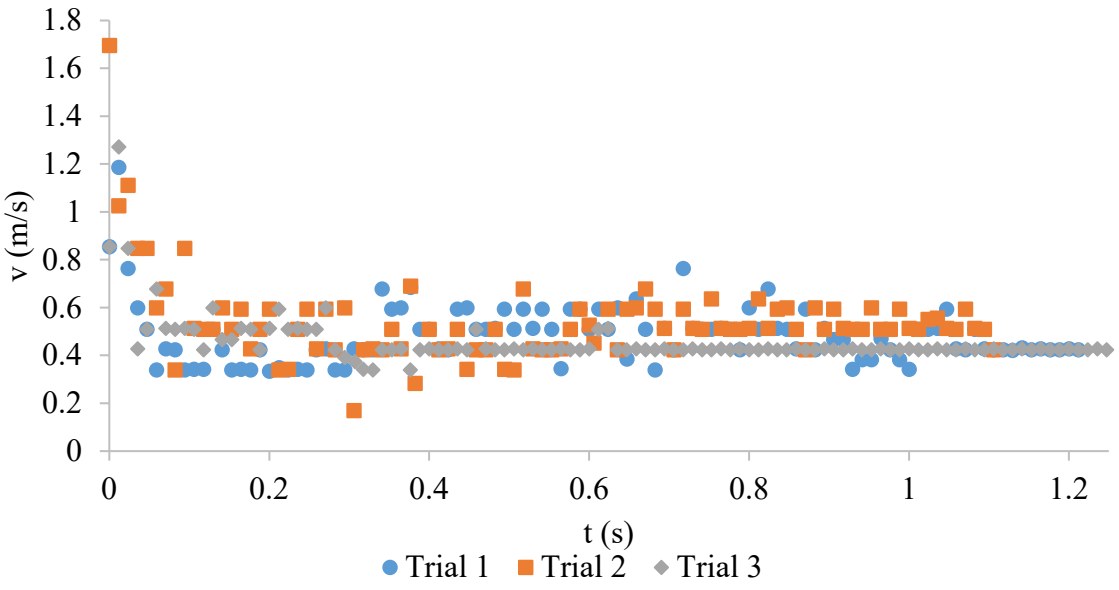

Figure 23: 4.76 mm diameter instantaneous velocity vs time for 0.1% Flowzan, 3% NaCl.

Using the instantaneous velocity obtained, as shown in Figure 23, the Reynolds number and the coefficient of drag were calculated using Equation 11, the particle parameters, and drag force respectively. Figure 24 shows the coefficient of drag vs. Reynolds number graph for the 4.76 mm sphere in 0.1 % Flowzan and 3 % NaCl. From this graph, a power relationship was found to fit best the relationship between the drag coefficient and Reynolds number.

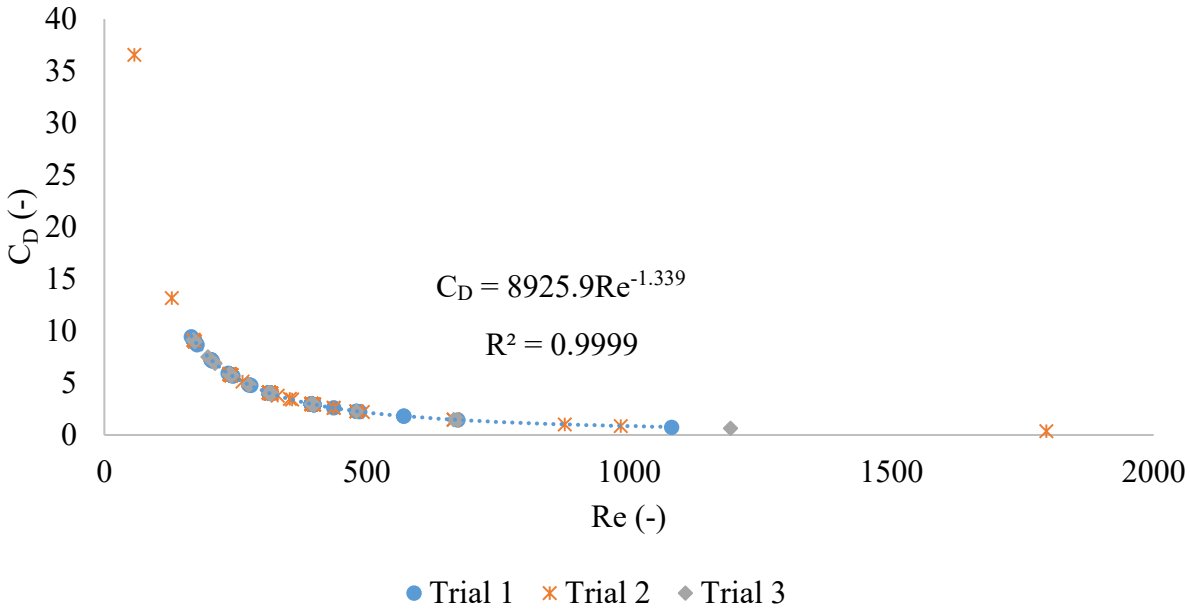

Figure 24: Coefficient of drag vs. Reynold number graph for 4.76 mm diameter sphere in 0.1% Flowzan, 3% NaCl fluid.

Similarly, the analysis was then conducted for the 9.53 mm diameter black glass ball. Figure 25 and Figure 26 presents the instantaneous velocity vs. time graph and the coefficient of drag vs. Reynold's number for the fluid with 0.1 % Flowzan and 3 % sodium chloride. Comparing the graphs of the two different diameter spheres, it was observed that there were more variations or fluctuations in the data point for the larger diameter ball. This behavior can be due to the wall effect being more prominent on a larger sphere. Also, it was observed that the coefficient of drag vs. Reynold's number plot for both the spheres was similar in trend.

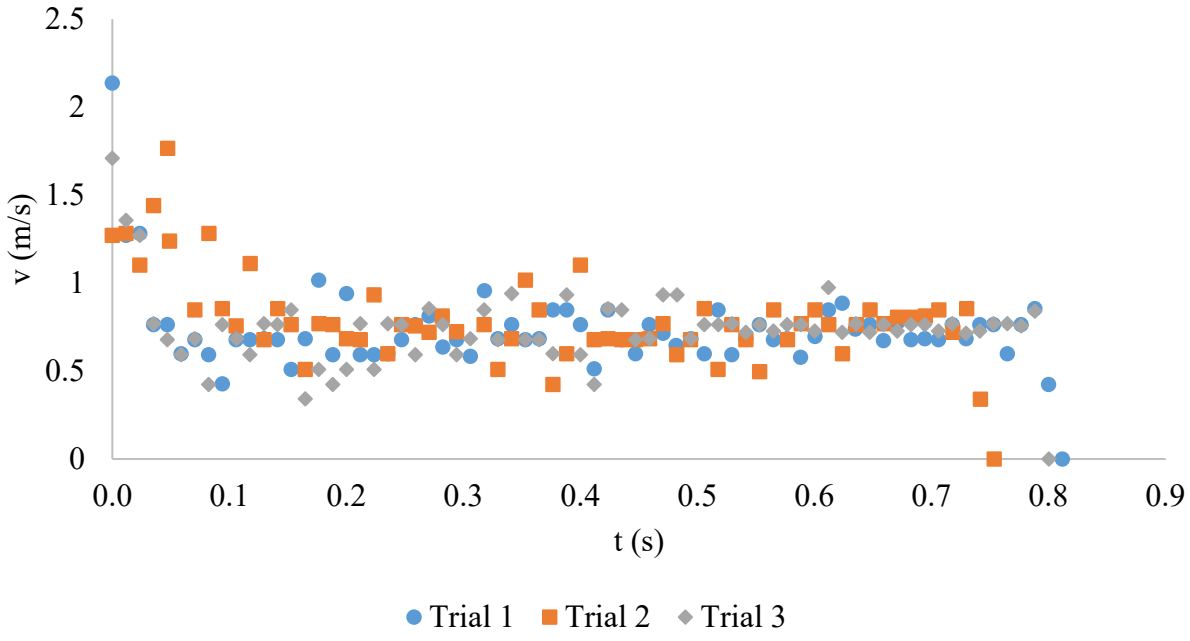

Figure 25: 9.53 mm diameter instantaneous velocity-time graph for 0.1% Flowzan, 3% NaCl.

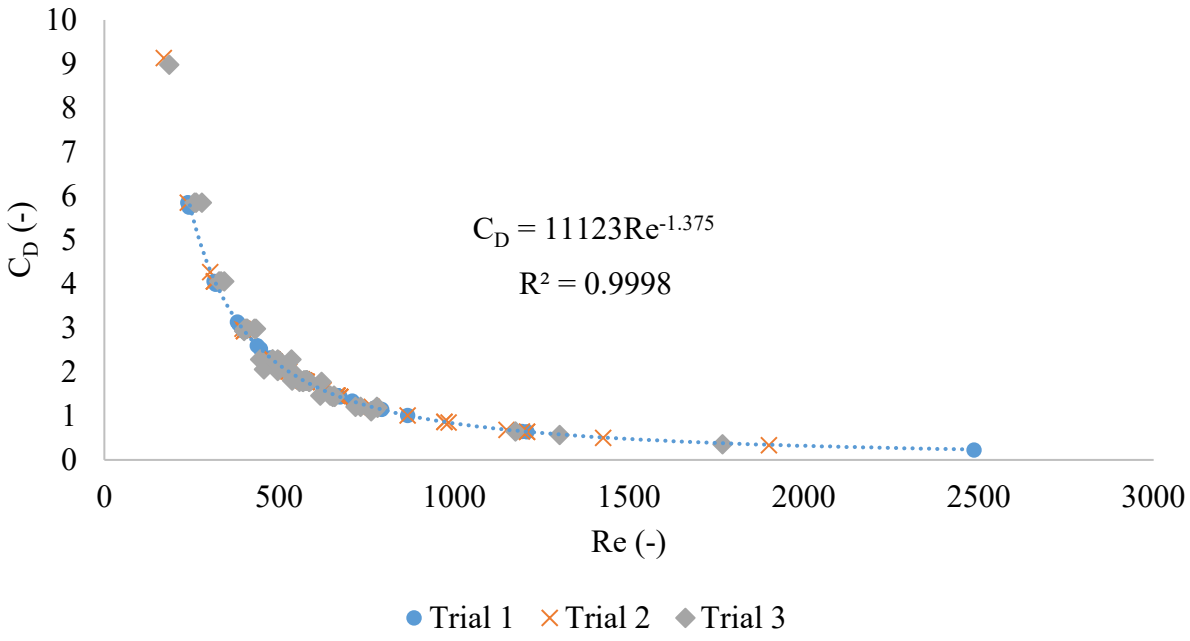

Figure 26: Coefficient of drag vs. Reynold number graph for 9.53 mm diameter sphere in 0.1% Flowzan, 3% NaCl fluid.

The next fluid that was analyzed was the 0.1 wt% Flowzan and 9wt% NaCl. Figure 27 shows the instantaneous velocity vs. time graph for the 4.76 mm sphere in a fluid of 0.1 % Flowzan and 9 % NaCl. In comparison to the previous graphs, it was observed that an increase in

the salt concentration resulted in a decrease of the terminal velocity, as seen in the case of the 9.53 mm diameter sphere, as shown in Figure 28.

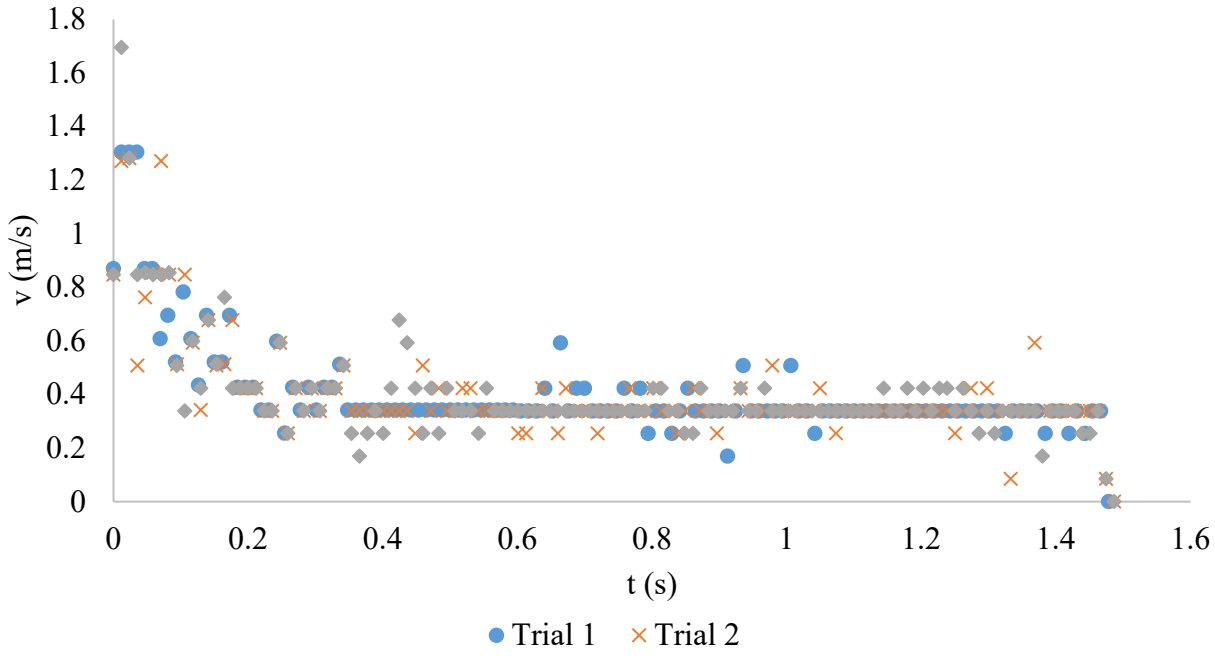

Figure 27: 4.76 mm diameter instantaneous velocity vs time for 0.1% Flowzan, 9% NaCl.

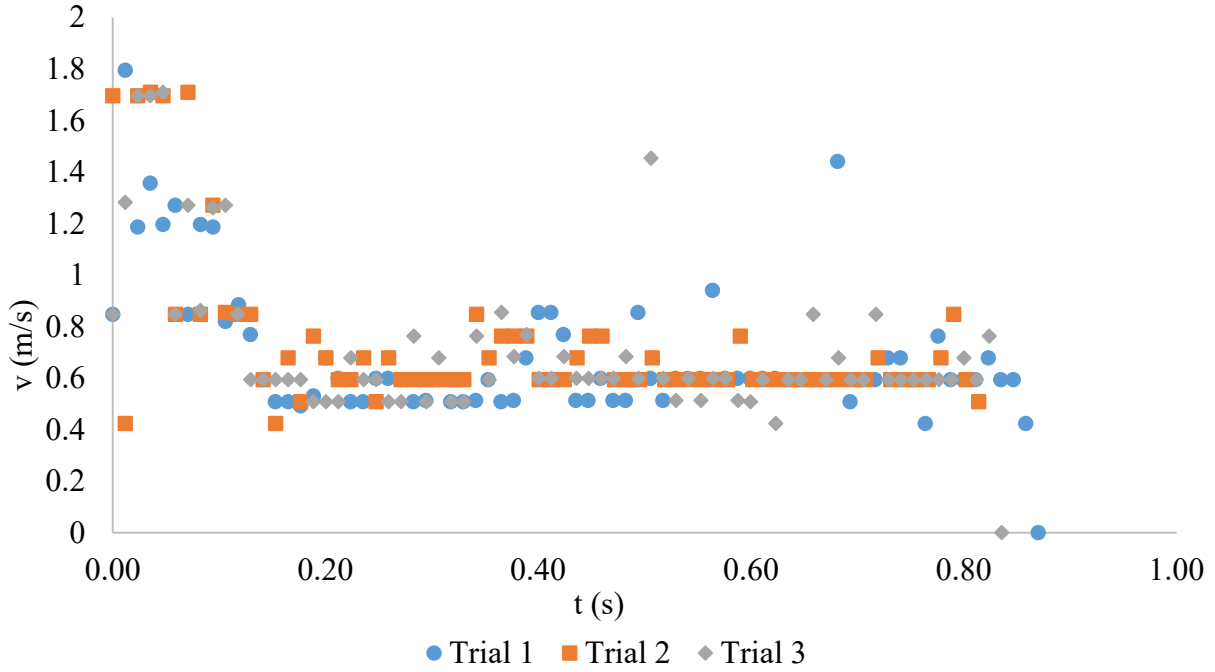

Figure 28: 9.53 mm diameter instantaneous velocity vs time for 0.1% Flowzan, 9% NaCl.

To observe the effect of change in the diameter of the ball, a terminal velocity vs. diameter of the glass ball graph was plotted for two different fluids to observe the effect of changing ball diameter on the terminal velocity. The graph in Figure 29 presents that an increase in ball diameter increases terminal velocity. Similarly, if the Flowzan percentage is kept the same and the percentage of NaCl salt increases, this causes an increase in terminal velocity as well.

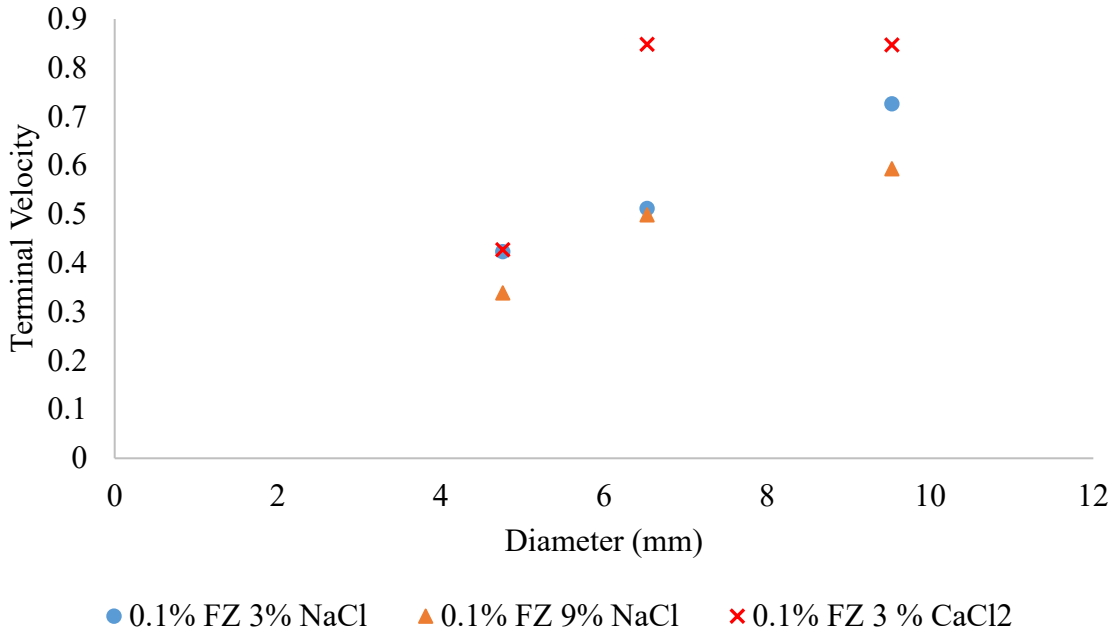

Figure 29: Terminal velocity vs., glass ball sphere diameter graph.

Next, the terminal velocity determined from the velocity-time graph of the different sized diameter sphere balls was plotted against the viscosity of the different fluids. Figure 30 presents the terminal velocity of the particles against the viscosity of the fluids.

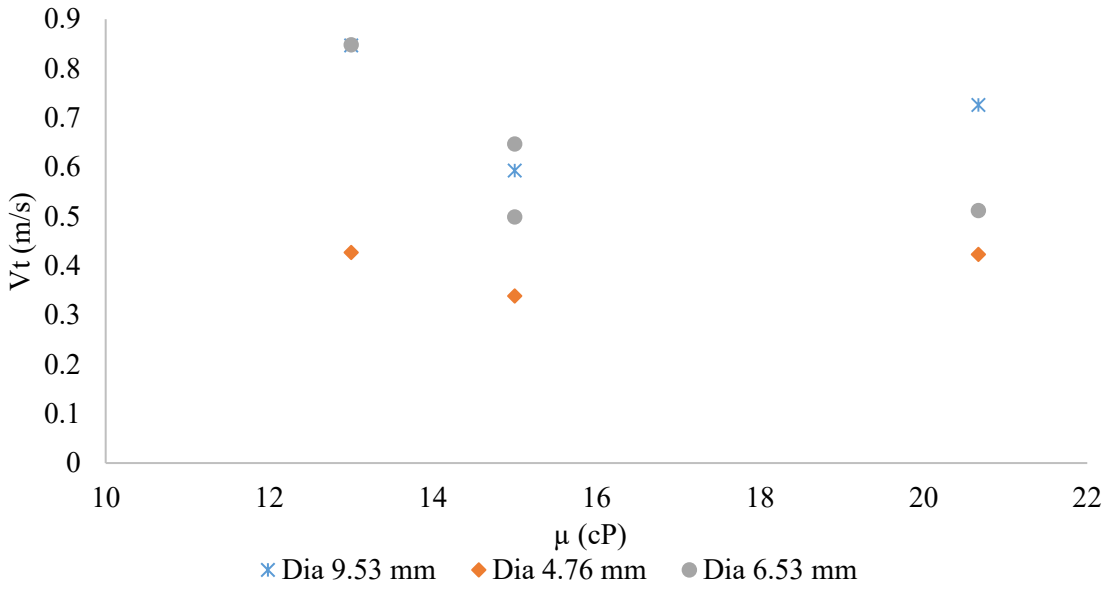

Figure 30: Terminal velocity against the viscosity of the fluid.

No clear trend was observed between the terminal velocity and the viscosity of the fluid, as seen in Figure 30. Possible reasons for such a phenomenon to occur was that the diameter of the spheres is too small for the effect of different viscosity of the fluids to be shown. Another possible reason could be that as the viscosities of the fluids were close to one another, the effect on the terminal velocity may not be noticeable.

Non-spherical Particle in Non-Newtonian Fluid

For further investigation, the particle shape was changed from spherical to irregular shaped particles to represent the particles in real life. The particles were collected randomly from outside to test different types of rocks found. Initially, the radius of the particle had to be approximated. First, the method of submerging the rock into the water and determining the change in volume was tested. However, as the particle was small, the change in water level was not noticeable between the different particles. Hence this method was not found to be effective.

From the literature review, a method of determining the Feret diameter was found, which involved taking pictures of rock from different angles. The pictures would then be uploaded on software, which would calculate the approximate diameter of the rock. However, when the software was used the values for the diameter found did not look like reasonable estimates. For example, for two rocks, the diameter was found to be two times smaller than the smallest side rock. Finally, the method that was used to approximate the diameter of the rock was through using a formula found during research. New pictures were taken with a ruler that had small increments next to the rock. Using a computer to blow up the images, the shorted and longest length of the rock was recorded. These lengths were put into the formula to calculate the apparent diameter of the rocks.

The rocks were placed in the fluids for a week before they were used for experimentations, as it was observed that without this step, the rocks would break a little every time the rocks hit the bottom of the column. This would cause the results to be unreliable as the rocks properties such as mass are not constant between the trials. For each rock, a velocity-time graph was plotted, as shown in Figure 31.

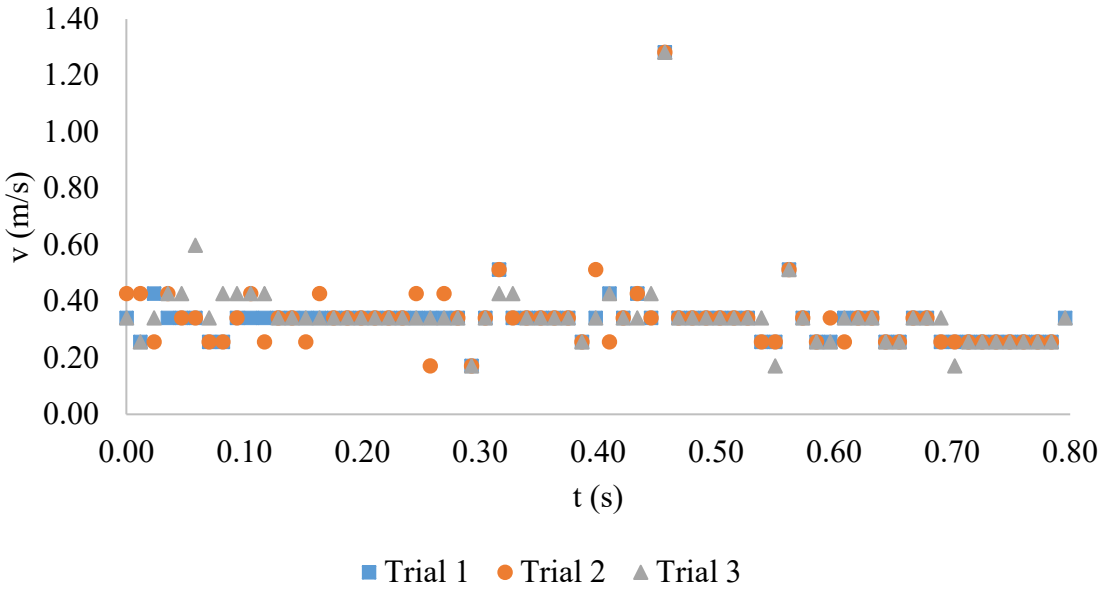

Figure 31: Rock 1: 0.1 % FZ & 9 % NaCl.

The above graph shows that the velocity of the rocks is around the same value. The fluctuations are due to the change in orientation of the rock. In some cases, the rock would hit the wall of the column causing its velocity to change. Also, any air bubbles in the fluid would affect the trajectory and hence the speed of the particle as it fell through the fluid. A similar trend was obtained for the other rocks. The settling velocity was recorded from these graphs.

Next, the drag coefficient vs. Reynold's number was plotted for the rocks in different fluids. Figure 32, Figure 33, and Figure 34 present the drag coefficient vs. Reynold's number graph for the same rock in three different fluids.

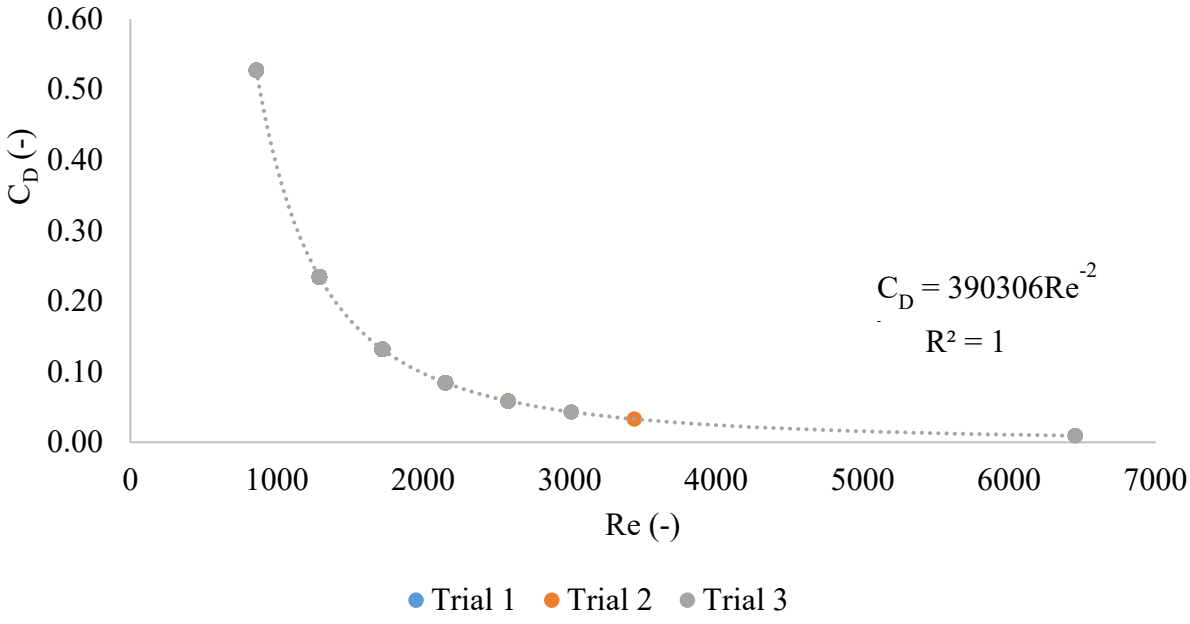

Figure 32: Rock 1: 0.1 % FZ & 9 % NaCl.

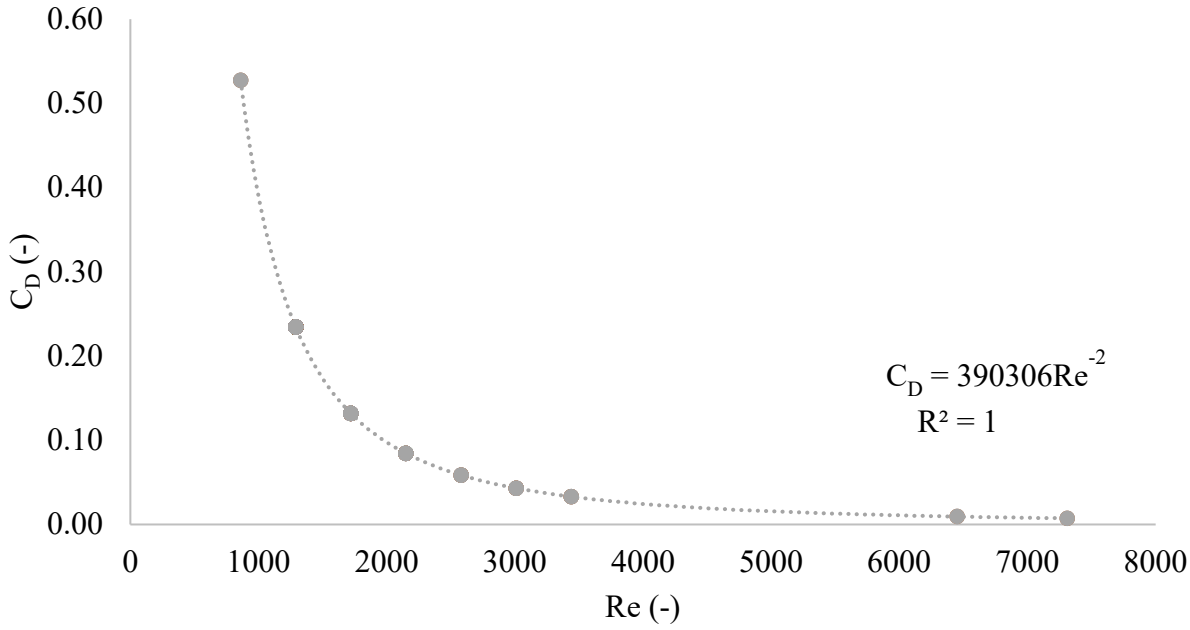

Figure 33: C_D vs Re for rock particle in 0.2 % Flowzan & 9 % NaCl.

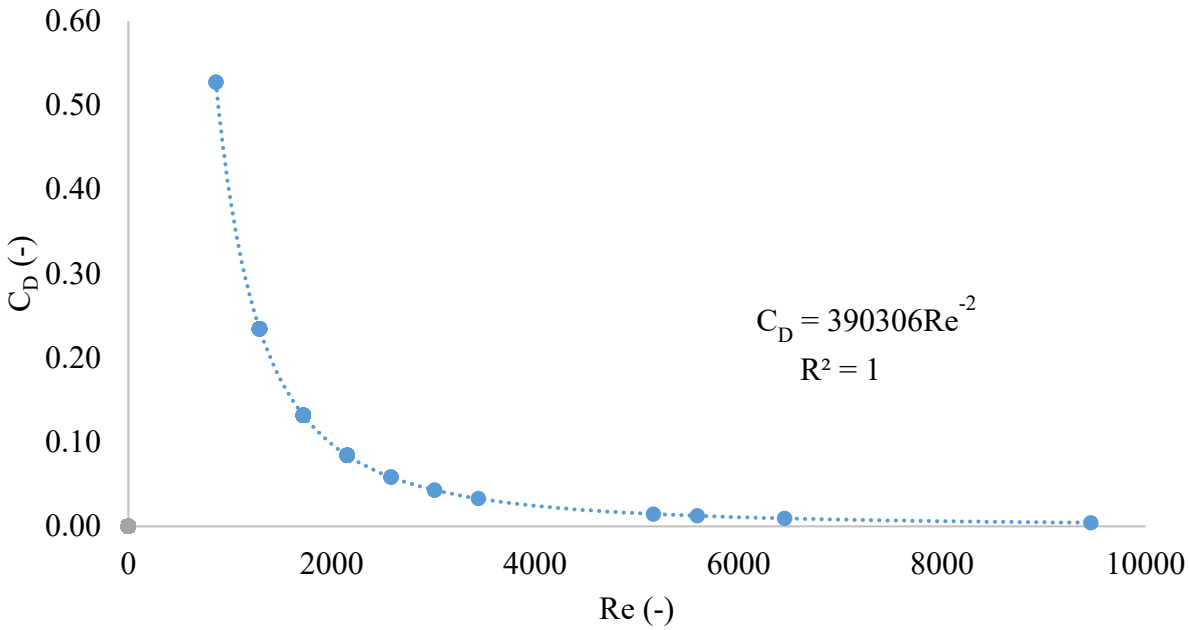

Figure 34: C_D vs Re for rock particle in 0.2 % Flowzan & 3 % $CaCl_2$.

From the graphs above, it is deduced that there is a power relationship between the drag coefficient and Reynold's number for non-spherical particles in non-Newtonian fluids containing Flowzan and salts. The equation was the same for the same rock in different fluids. Comparing it to the data obtained from other non-spherical particles, a power relationship was still observed. The only thing that changes is the coefficient in front of Re^{-2}. From this, it can be concluded that the particles move similarly in different non-Newtonian fluid, but each particle differs from one another. This means that to determine the settling velocity of a particle, its shape and size must be known.

To determine the relationship between the sphericity of the particles and the settling velocity, the Sneed and Folk method was used to calculate the sphericity of the non-spherical particles. Equation 15 was used to calculate the sphericity where s is the short axes, l is the long axes, and i is the intermediate axes. The sphericities were plotted with the terminal velocities of some rocks in two different fluids. The plot is shown in Figure 35.

$$\psi = \left(\frac{s^2}{li}\right)^{\frac{1}{3}} \quad (15)$$

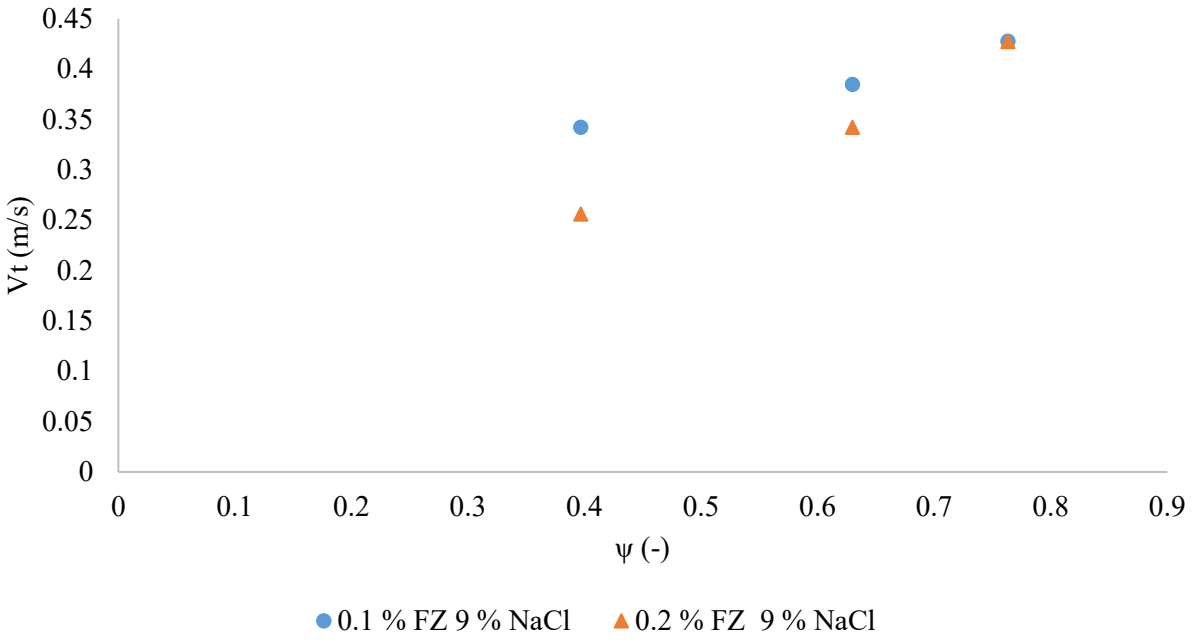

Figure 35: Terminal velocity of rock particles against their sphericities for two different fluids.

From the graph above, it is observed that as the sphericity of the particle increases, so does the terminal velocity. Also, it is shown that for non-spherical particles increasing the weight percentage of Flowzan reduces the terminal velocity of the particle.

CHAPTER IV

CONCLUSION

With limited literature available on settling velocity models for non-Newtonian Herschel Bulkley fluids, one of the aims of this project was to derive a model of settling velocity for these kinds of fluids.

From the experiments of settling velocity, which the team was able to conduct until the closure of the research lab in TAMUQ due to the COVID-19 crisis, the team was able to determine the settling velocity for fluids with different concentrations of Flowzan and different salt concentrations in the smaller acrylic column. It was observed that terminal velocity was achieved for the three different black balls of diameter 4.76 mm, 6.35 mm & 9.53 mm within the 60 cm of the non-Newtonian fluid column.

Following are the conclusions that were made from the experiments:

1. Larger spherical particles had a higher terminal velocity.
2. There was an increase in the terminal velocity for solutions with higher percentages of salt concentration.
3. There is a power relationship between the drag coefficient and the Reynold's number for the non-Newtonian fluid containing Flowzan and salts.
4. The terminal velocity of particles with larger sphericity will be higher than the particles with smaller sphericity.
5. Increasing the weight percentage of Flowzan for non-spherical particles decreases the terminal velocity of the particle.

For future work, the investigation of molecular properties of both NaCl and $CaCl_2$ would provide a better insight into the optimal concentrations of each salt as well as the current results of the project. Another task that could be done in the future would include conducting the same experiments at a higher temperature to develop a better understanding of the rheology of the drilling fluids in order to imitate the nature of the fluid that would be typically found in Qatar.

Due to the unforeseen events surrounding the COVID-19 virus in spring 2020, all experimentations at the time of publication for this URS thesis were not completed. The following areas should be explored for future research:

- Effect of column size on the settling velocity of particles.
- Effect of temperature of the fluid on the settling velocity of the particles.
- Carry out more trials to confirm data.
- Do experiments with particles larger than 3 cm in diameter.

REFERENCES

[1] Inc, “Viscosity of Newtonian and Non-Newtonian Fluids,” Viscosity of Newtonian and Non-Newtonian Fluids. [Online]. Available: https://www.rheosense.com/applications/viscosity/newtonian-non-newtonian. [Accessed: 08-Nov-2019].

[2] Melton, L. L., & Saunders, C. D. (1957, January 1). Rheological Measurements of Non-Newtonian Fluids. Society of Petroleum Engineers.

[3] Gucuyener, I. H. (1983, January 1). A Rheological Model for Drilling Fluids and Cement Slurries. Society of Petroleum Engineers. doi:10.2118/11487-MS

[4] J. Hassiba, Khaled & Amani, Mahmood. (2012). The Effect of Salinity on the Rheological Properties of Water Based Mud under High Pressures and High Temperatures for Drilling Offshore and Deep Wells. Earth Science Research. 2. 10.5539/esr.v2n1p175.

[5] Anawe, Paul & Folayan, Adewale. (2019). Advances in drilling fluids rheology.

[6] “Settling Velocity,” *Settling Velocity - an overview | ScienceDirect Topics*. [Online]. Available: https://www.sciencedirect.com/topics/earth-and-planetary-sciences/settling-velocity.

[7] Abdelkrim, Hazzab & Terfous, Abdelali & Ghenaim, Abdellah. (2008). Measurement and modeling of the settling velocity of isometric particles. Powder Technology. 184. 105-113. 10.1016/j.powtec.2007.08.009. https://www.researchgate.net/publication/229102627_Measurement_and_modeling_of_the_settling_velocity_of_isometric_particles.

[8] Concha, Fernando. (2009). Settling Velocities of Particulate Systems. KONA-POWDER AND PARTICLE. 27. 18-37. 10.14356/kona.2009006. http://www.researchgate.net/publication/234102487_Settling_Velocities_of_Particulate_Systems

[9] AmbiValue, Application note 2017.03 https://www.ambivalue.com/site/assets/files/1017/eyetech-application-note-2017_03.pdf

[10] H. Moes, R. Flash; Ankersmid, Advances in Particle Size Analysis by Laser Obscuration Time Combined technologies for particle size, shape and concentration measurement, ANKERSMID International http://www.rktech.hu/dokumentaciok/AmbiValue/Poster/EyeTech_Poster.pdf

[11] M. A. R. Mohammed, "Studying the Factors Affecting the Settling Velocity of ...," 2013. [Online]. Available: https://www.iasj.net/iasj?func=fulltext&aId=86463. [Accessed: Feb-2020]

[12] V. Kelessidis and G. Mpandelis, "Measurements and prediction of terminal velocity of solid spheres falling through stagnant pseudoplastic liquids," Powder Technology, vol. 147, no. 1-3, pp. 117–125, 2004.

[13] N.-S. Cheng, Comparison of formulas for drag coefficient and settling velocity of spherical particles, Powder Technol. 189 (2009) 395–398

[14] S. Rushd, I. Hassan, R. A. Sultan, V. C. Kelessidis, A. Rahman, H. S. Hasan, and A. Hasan, "Terminal settling velocity of a single sphere in drilling fluid," Particulate Science and Technology, pp. 1–10, 2018

[15] Wilson, K. C., R. R. Horsley, T. Kealy, J. A. Reizes, and M. Horsley. 2003. Direct prediction of fall velocities in non-Newtonian materials. International Journal of Mineral Processing 71 (1–4):17–30, 2003

[16] A. Margaritis, D. W. T. Bokkel, and D. G. Karamanev, "Bubble rise velocities and drag coefficients in non-Newtonian polysaccharide solutions," Biotechnology and Bioengineering, vol. 64, no. 3, pp. 257–266, 1999